Available online at www.sciencedirect.com
SCIENCE DIRECT®
Electrochimica Acta 50 (2005) 2893–2904
ELECTROCHIMICA Acta
www.elsevier.com/locate/electacta

Synthesis and characterization of nickel tungsten alloys by electrodeposition

N. Eliaz[a,*], T.M. Sridhar[a], E. Gileadi[b]

[a] *Biomaterials and Corrosion Laboratory, Department of Solid Mechanics, Materials and Systems, Tel-Aviv University, Ramat-Aviv 69978, Israel*
[b] *School of Chemistry, Raymond and Beverly Sackler Faculty of Exact Sciences, Tel-Aviv University, Ramat-Aviv 69978, Israel*

Received 9 August 2004; received in revised form 10 November 2004; accepted 13 November 2004
Available online 18 December 2004

Abstract

The objective of the current work was to study in detail the effect of bath chemistry, additives and operating conditions on the chemical composition, microstructure and properties of Ni–W alloys deposited from citrate-containing baths, in the absence of ammonia or ammonium salts, on stationary working electrodes. The morphology of the deposits was studied by scanning electron microscopy (SEM) as well as atomic force microscopy (AFM), and the approximate composition by energy dispersive spectroscopy (EDS). Metallographic cross-sections were also analyzed, and micro-hardness tests conducted. The results are discussed in detail with emphasis on routes to increase the tungsten content and deposit thickness, while reducing the extent of cracking.

Keywords: Nickel–tungsten alloys; Amorphous alloys; Electrodeposition; Anomalous codeposition

1. Introduction

The interest in electrodeposition of nickel–tungsten (Ni–W) alloys has increased in recent years due to their unique combination of tribological, magnetic, electrical and electro-erosion properties. These alloys exhibit good mechanical properties (e.g., high tensile strength and premium hardness, as well as superior abrasion resistance), good resistance to strong oxidizing acids, and high melting temperature [1–5]. It was reported [6], for example, that the corrosion rate of an amorphous Ni–W deposit in hydrochloric acid at 30 °C is only 1/40 that of type 304 stainless steel (UNS S30400) commonly used in industry. In general, the passivation current density (i_{pass}) drops remarkably with the addition of tungsten to nickel [6]. While the hardness of the as-plated alloy is typically in the range 650–750 VHN, baking heat treatment at temperatures ranging from 190 to 600 °C for 12–24 h can raise it to 1200–1400 VHN [7,8].

Current and possible future applications of Ni–W alloys include barrier layers or capping layers in copper metallization for ultra-large-scale integration (ULSI) devices or microelectromechanical systems (MEMS), mold inserts, magnetic heads and relays, bearings, resistors, electrodes accelerating hydrogen evolution from alkaline solutions, environmentally safe substitute for hard chromium plating in the aerospace industry, etc. [1–13].

It is well known that tungsten cannot be electrodeposited from an aqueous solution of sodium tungstate (Na_2WO_4) or any other soluble compound containing this element. However, if a suitable nickel compound such as nickel sulfate ($NiSO_4$) is added to the plating bath, induced codeposition can take place, forming Ni–W alloys. A similar phenomenon is observed during electrodeposition of W, Mo or Re with Ni, Co or Fe, as well as in electroless deposition of Ni–P

* Corresponding author. Tel.: +972 3 640 7384; fax: +972 3 640 7617.
E-mail address: neliaz@eng.tau.ac.il (N. Eliaz).

0013-4686/$ – see front matter © 2004 Elsevier Ltd. All rights reserved.
doi:10.1016/j.electacta.2004.11.038

or Co–P alloys. Ammonia (NH_3) is also frequently added to Ni–W plating baths to increase the Faradaic efficiency (FE) and fine-tune the pH, while sulfuric acid (H_2SO_4) and sodium hydroxide (NaOH) are added to adjust the pH, typically within the range of 7.0–9.0. Organic acids such as citric, tartaric, malic, gluconic, saccharic or hydroxyl acetic acids are used to improve the FE and the solubility of the metal ions in the bath [10]. These baths are usually operated at an elevated temperature of 50–80 °C.

The tungsten content of the alloy is usually in the range of 5–25 at.% (13–50 wt.%). One of the commercial plating solutions (ENLOY® Ni-500 from Enthone), for example, yields 35–40 wt.% tungsten in the deposit [7]. In order to further improve the tribological properties and thermal stability of the coating, it is sometimes desirable to increase its tungsten content. Unfortunately, this has been found difficult, even when the WO_4^{2-} ion in solution is in large excess compared to the Ni^{2+} ion [1]. One possible way to increase the tungsten concentration in the alloy is to apply periodic current reverse pulse plating, which may also increase the throwing power and the deposition rate, as well as improve the properties of the deposit (e.g., reduce residual stresses and porosity, refine the grain size, improve wear and corrosion resistance, etc.) [11,14].

Another route has recently been suggested by Gileadi and co-workers [1–5], who developed a novel plating bath for codeposition of Ni–W alloys with high tungsten content. By removing the NH_3 from the bath and using citrate $(C_6H_5O_7)^{3-}$ as a ligand, the tungsten content of the alloy could be increased to 50 at.% (76 wt.%). The working hypotheses in the above studies are that (a) the tungstate/citrate complex forms a complex with nickel citrate in the bulk of the solution or on the surface; (b) this ternary complex, of the type $[(Ni)(HWO_4)(Cit)]^{2-}$, is the precursor for the deposition of the Ni–W alloy; (c) nickel can also be deposited from its complexes with either citrate or NH_3. The overall reaction of the ternary complex requires eight electrons and can be written as:

$$[(Ni)(HWO_4)(Cit)]^{2-} + 8e^- + 3H_2O \rightarrow NiW + 7(OH)^- + Cit^{3-} \quad (1)$$

In the previous work of Gileadi and co-workers, a rotating gold cylinder served as the working electrode. Such working electrodes, however, are impractical for industrial use. Furthermore, it is well known that codeposition of nickel and tungsten is very sensitive to changes in operating conditions. In spite of this, no additives were used in the previous work in order to keep the system as simple as possible, and mainly one current density of 15 mA cm^{-2} was applied. Thus, the objective of the current work is to study the effect of operating conditions and bath additives on the Faradaic efficiency, chemical composition, surface morphology, thickness and hardness of nickel–tungsten alloys deposited on stationary working electrodes in open baths.

2. Experimental

2.1. Plating bath chemistry

Nickel–tungsten alloys were electroplated from aqueous solutions containing $NiSO_4 \cdot 6H_2O$ (nickel sulfate hexahydrate, Merck #06727, 0.01–0.10 M) and $Na_2WO_4 \cdot 2H_2O$ (sodium tungstate dihydrate, Fluka #72070, 0.40 M) as the electroactive species, and $C_6H_5Na_3O_7 \cdot 2H_2O$ (tri-sodium citrate dihydrate, Merck #06448, 0.25–0.60 M) as the complexing agent. It should be noted that in contrast to previous work, the bath chemistry was selected in certain experiments so that the sum of the molar concentrations of $NiSO_4$ and Na_2WO_4 exceeded that of Na_3Cit. All reagents were dissolved in Simplicity™ water (Millipore, resistivity 18.2 MΩcm). The pH was measured by means of InoLab pH/Oxi Level 3 meter from WTW and adjusted to a value of 8.0 through additions of H_2SO_4 and NaOH.

The effect of several bath additives was studied. Nickel sulfamate, $Ni(NH_2SO_3)_2$, is a salt of the strong monobasic sulfamic acid (NH_2SO_3H). Its incorporation in nickel (and other) plating baths has been reported to result in higher deposition rates attainable, superior throwing power, lower power requirements, as well as reduced porosity and reduced residual stresses in the deposit [15,16]. In this work, $Ni(NH_2SO_3)_2 \cdot 4H_2O$ (nickel(II) sulfamate tetrahydrate, Aldrich Chemical #26,227-7, 20–40 g L^{-1}/62–124 mM) was added to the bath in several experiments.

Saccharin ($C_7H_5NO_3S$) is a surface-active organic compound that has been reported to reduce the residual tensile stresses, refine the grain size and increase the hardness, tensile strength and ductility of electrodeposited nickel [16–18]. Saccharin is likely to increase also the allowable deposition rate of nickel due to the electron withdrawing group (the aromatic ring) of this molecule, which may affect the FE. This additive is generally used in nickel electroplating as sodium saccharin salt ($NaC_7H_4NO_3S$) at a concentration of 0.5–4.0 g L^{-1} (2.4–19.5 mM) [19]. Thus, 14.6 mM saccharin (Sucrazit, Biscol; contains 23.81 wt.% sodium saccharin, the rest being sodium bicarbonate and fumaric acid) was added in the present work to several plating baths.

Chloride ions are added to commercial nickel sulfate (and other) baths in order to reduce the polarization and prevent passivation of the anodes. One possible explanation is that the strongly coordinating chloride forms a complex with nickel, which might otherwise have formed a passive film. While the residual tensile stresses in the deposit usually rise with increasing concentrations of chloride, the plating process is enhanced due to increased bath conductivity, increased cathode and anode efficiencies, and hence increased throwing power [16]. In the current work, NaCl (sodium chloride, Merck #06404, 2–5 mM) was added to some of the baths.

Ammonium sulfate ($(NH_4)_2SO_4$) has been reported to increase the current efficiency in several electroplating

systems, including rhenium [20]. However, in order to avoid any complexing effects of ammonium in our system, the effect of Na_2SO_4 (sodium sulfate anhydrous, Frutarom, 25 g L^{-1} /176 mM) additions was evaluated in this work instead. Gelatin is also sometimes added to electroplating baths to control the deposition rate, crystallization, leveling and brightness of the deposit (e.g., in zinc electrodeposition [21]). In the current work, gelatin (Fluka #48720, 0.5–1 wt.%) was added to certain baths.

2.2. Operating conditions

In this work, a two-electrode cell was used. A sheet of gold with an exposed area of 1 cm^2 was used as the cathode. The reason for this selection was to eliminate the effect of substrate chemistry and surface condition when comparing to the previous studies of Gileadi et al., which were carried out with a cylindrical rotating gold electrode. A platinum mesh was used as the anode and was placed 10 mm away from the cathode. The anode-to-cathode surface area ratio was approximately 4.4, high enough to prevent polarization of the anode and an increase in the voltage drop between the two electrodes. A Keithley model 2425 Source Meter was used to control the applied current density at values of 5, 10 or 15 mA cm^{-2}. It may be noted that these values are lower than the ones commonly reported in the literature (see, for example, Refs. [9,14,22–24]). The Faradaic efficiency was calculated from the charge passed, the weight gained, and the chemical composition of the deposit, as determined by energy dispersive spectroscopy (EDS), using the following equation:

$$\mathrm{FE} = \frac{w}{It} \sum \frac{c_i n_i F}{B M_i} \times 100 \quad (2)$$

where w is the measured weight of the deposit (g), I is the current passed (A), t is the deposition time (h), c_i is the weight fraction of the element (either nickel or tungsten) in the binary alloy deposit, n_i is the number of electrons transferred in the reduction of 1 mol atoms of that element ($n_i = 2$ for nickel and 6 for tungsten), M_i is the atomic weight of that element (g mol^{-1}), F is the Faraday constant (96,485.3 C mol^{-1}) and B is a unit conversion factor (3600 C $A^{-1}h^{-1}$).

Before turning on the current, the bath was purged with purified nitrogen for about 15 min. Purging at a lower nitrogen partial pressure continued during deposition. In most cases, the plating bath was operated at room temperature. However, some experiments were carried out at different temperatures from 30 to 70 °C. A Lauda Ecoline E-220T thermostatic bath was used to control the temperature at ±0.01 °C. Finally, in order to maintain the homogeneity of solution and reduce pitting due to accumulation of hydrogen at the surface of the cathode, vigorous agitation at 1500 rpm was applied in all baths. To this aim, a Maxi S flat magnetic stirrer with Telemodul 40S controller from H + P was used. The electroplating process was typically run for 6 h (which implies, for example, a charge of 324 C transferred at I = 15 mA).

2.3. Characterization techniques

The morphology of the deposits after drying was observed with a scanning electron microscope (SEM, Jeol model JSM-6300). The attached energy dispersive spectroscopy (EDS, Oxford Isis system) was used to determine the approximate composition of the alloy. Several sessions were carried out with a field-emission high-resolution SEM (Jeol model JSM-6700F). The thickness of the deposit was large enough so that no signal from the underlying gold substrate was observed. Each sample was measured at different locations to confirm uniformity. Optical microscopy (Olympus IX71) was used to study both the macro-structure and thickness of deposits. Ex situ atomic force microscopy (AFM, using Molecular Imaging model PicoSPM™ operated under contact mode) was also used to analyze the structure of the deposits at near-atomic resolution. The hardness of selected deposits was measured on metallographic cross-sections by means of the Vickers micro-hardness technique under a load of 10 g.

3. Results and discussion

In the framework of this work, over 100 samples were coated under different bath chemistries and operating conditions and were characterized. In Section 3.1, the effects of concentration of nickel and citrate ions on the FE and tungsten content in the deposited alloy are discussed. Subsequently, Section 3.2 shows the effects of different bath additives on the FE and tungsten content. The effects of bath temperature and current density are discussed in Sections 3.3 and 3.4, respectively. Finally, the morphology, cracking pattern and hardness of representative coatings are analyzed in Section 3.5.

3.1. The effect of the concentration of nickel and citrate ions in the bath

In Section 2.1 it was noted that all plating baths consisted of nickel sulfate, sodium tungstate and tri-sodium citrate. Fig. 1a shows the effect of changing the concentration of nickel ions in the bath on the FE and coating tungsten content at different current densities. Note that the solid symbols refer to the FE values, while the same empty symbols refer to values of the tungsten content. In all cases the concentrations of the tungstate and citrate ions in the bath were 0.40 and 0.50 M, respectively. The FE is seen to increase with the concentration of Ni^{2+} and decrease with increasing current density. The nickel content of the bath also affected tungsten content in the deposit. While the tungsten content fell within the range 30–35 at.% (58–63 wt.%) for both the 0.05 M Ni^{2+} and the 0.10 M Ni^{2+} baths at all current densities, it increased significantly to 60–75 at.% (83–90 wt.%) for the 0.01 M Ni^{2+} bath. However, this is associated with very low FE and reflects a poor thin tungsten-based deposit rather than a good Ni–W deposit.

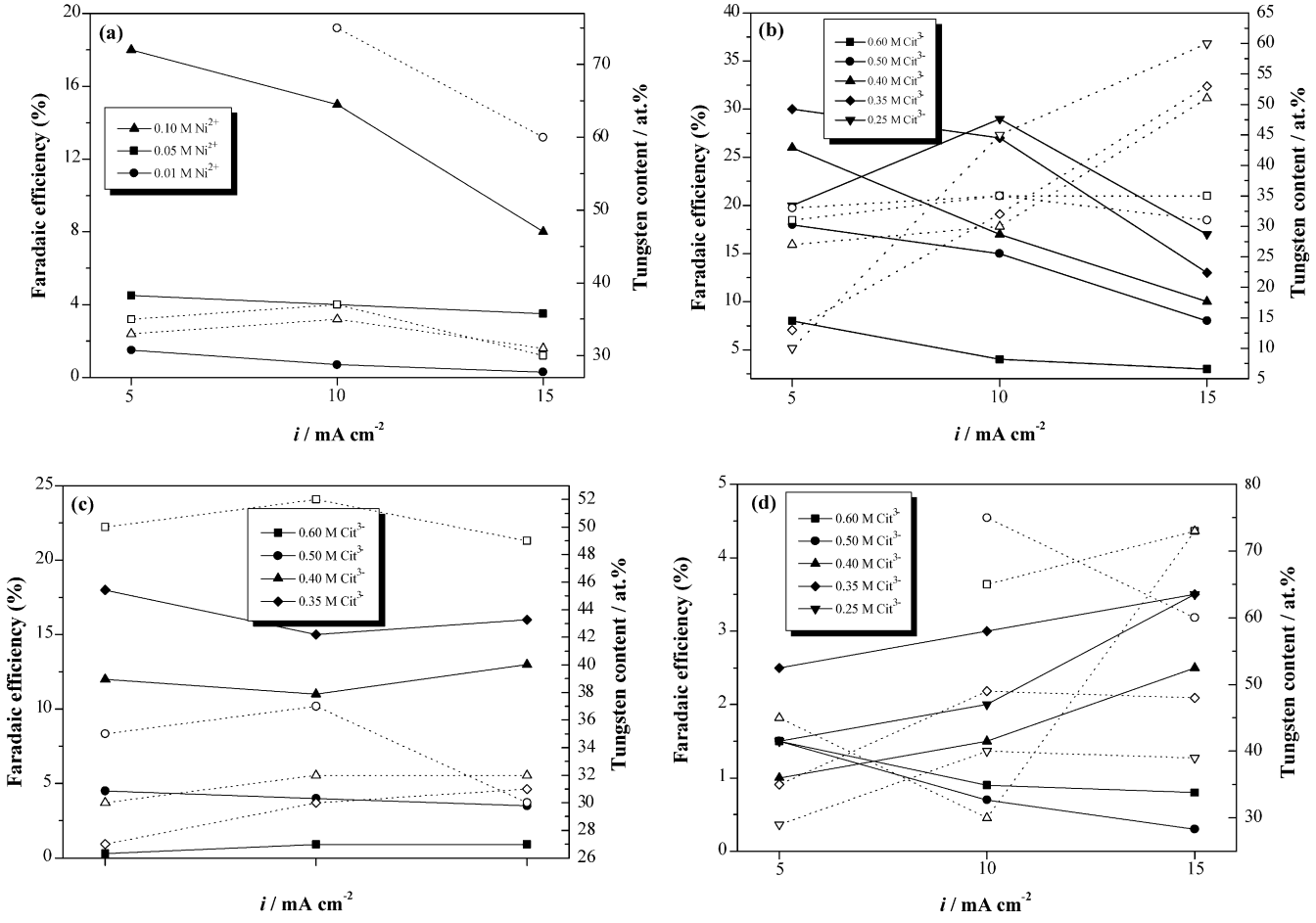

Fig. 1. The dependence of Faradaic efficiency (solid symbols, solid lines) and the tungsten content of the deposit (empty symbols, dot lines) on current density as well as on nickel ions concentration (a) and citrate ions concentration (b–d). The citrate ions concentration in (a) is 0.50 M. The nickel ions concentration is 0.10 M in (b), 0.05 M in (c), and 0.01 M in (d). Other variables, including tungstate ions concentration (0.40 M), absence of bath additives, plating period (6 h), nitrogen purging, and room temperature were kept constant.

For comparison, Younes and Gileadi [1] reported a maximum Faradaic efficiency of 11% and a maximal tungsten content of ∼67 at.% in two different baths containing different concentrations of Na_2WO_4. An increase in the bath concentration of Ni^{2+} has also been reported to cause a dramatic increase in the FE [3,24]. Furthermore, it has been reported that an increase in the concentration of Ni^{2+} results in an increase in the rate of both Ni and W deposition [14,25], but the tungsten content in the alloy decreases [5].

Fig. 1b shows the effect of the concentration of citrate ions on the FE and deposit tungsten content at various current densities. The concentrations of nickel and tungstate ions in the bath were 0.10 and 0.40 M, respectively. In general, the FE was found to decrease as the concentration of Cit^{3-} was increased. One should note the high FE (∼30%) that was attained at a low concentration of Cit^{3-} and a low current density.

From Fig. 1b it is noted that at a low current density (5 mA cm^{-2}), the tungsten content increased from 10 to 33 at.% (25–61 wt.%) as the concentration of Cit^{3-} was increased from 0.25 to 0.60 M. At a higher current density (15 mA cm^{-2}), however, the trend reversed and the tungsten content increased from 31 at.% (59 wt.%) to 60 at.% (83 wt.%) as the concentration of Cit^{3-} was decreased.

The effects of the citrate ion concentration on the FE and on the tungsten content in the deposit were studied for baths with different concentrations of Ni^{2+} too. Fig. 1c refers to a bath which contained 0.05 M Ni^{2+}, while Fig. 1d refer to a bath that contained 0.01 M Ni^{2+}. From Fig. 1c it is evident that the FE exhibits the same dependence on the Cit^{3-} concentration as reported above, namely the FE decreases with increasing Cit^{3-} concentration. The dependence is not as obvious when the concentration of Ni^{2+} is further decreased to 0.01 M (see Fig. 1d). In general, the tungsten content in the deposit was found to increase when the concentration of Cit^{3-} was increased in the 0.05 M Ni^{2+} bath (Fig. 1c), but this dependence became more complex when the concentration of Ni^{2+} was further decreased to 0.01 M (Fig. 1d). It should be emphasized that the high tungsten content measured in the last case for high citrate ion concentrations (see Fig. 1d) does not represent a good Ni–W coating. On these samples, extremely thin, non-adhesive deposits with poor coverage were

observed. In addition, the Ni–W phase diagram does not show formation of a NiW_3 intermetallic phase, which would correspond to the composition of 75 at.% shown in this figure.

It is well known that the tungsten content of the alloy depends, among others, on the type of the complexing agent used in the bath. Citrate baths have been reported to yield higher tungsten content than those containing tartrate or malate. However, an increase in the concentration of Cit^{3-} was sometimes found to result in a decrease both in the FE and in the tungsten content [5,14,26]. Huang [27], on the other hand, reported that addition of diammonium citrate to a sulfamate bath resulted in an increased concentration of tungsten in the alloy, but the residual stress was also increased. In a bath containing 0.10 M Ni^{2+} and 0.10 M WO_4^{2-}, Younes and Gileadi observed [3] that the tungsten content of the alloy increased when the concentration of Cit^{3-} was increased up to 0.50 M, but then started to decrease. The FE decreased dramatically when the concentration of citrate exceeded 0.20 M, i.e., when the molar concentration of citrate exceeded the sum of concentrations of nickel and tungstate ions. The deposition potential was observed to change in the negative direction with increasing citrate concentration, first sharply and then moderately. It was concluded that citrate, being a strong complexing agent for both nickel and tungsten ions, tends to sequester these ions in stable complexes, making it more difficult to deposit the alloy. The relative effect on nickel was found to be stronger up to a concentration of 0.50 M citrate and weaker at higher concentrations, leading to a maximum tungsten content at a Cit^{3-} concentration of about 0.50 M [3].

3.2. The effect of additives

The effect of several additives, namely nickel sulfamate, saccharin, sodium chloride, sodium sulfate and gelatin was studied. Fig. 2a shows the effect of nickel sulfamate on the FE of a bath containing 0.10 M Ni^{2+}, 0.40 M WO_4^{2-} and 0.50 M Cit^{3-} and on the deposit tungsten content. It may be noted that the FE increased with the addition of nickel sulfamate, the effect being more pronounced at high current densities. This increase in the FE was accompanied by a slight decrease in the tungsten content of the alloy, as seen in Fig. 2a. The structure of the coating, observed by SEM, did not change significantly as a result of nickel sulfamate addition. However, metallographic cross-sections did show a remarkable

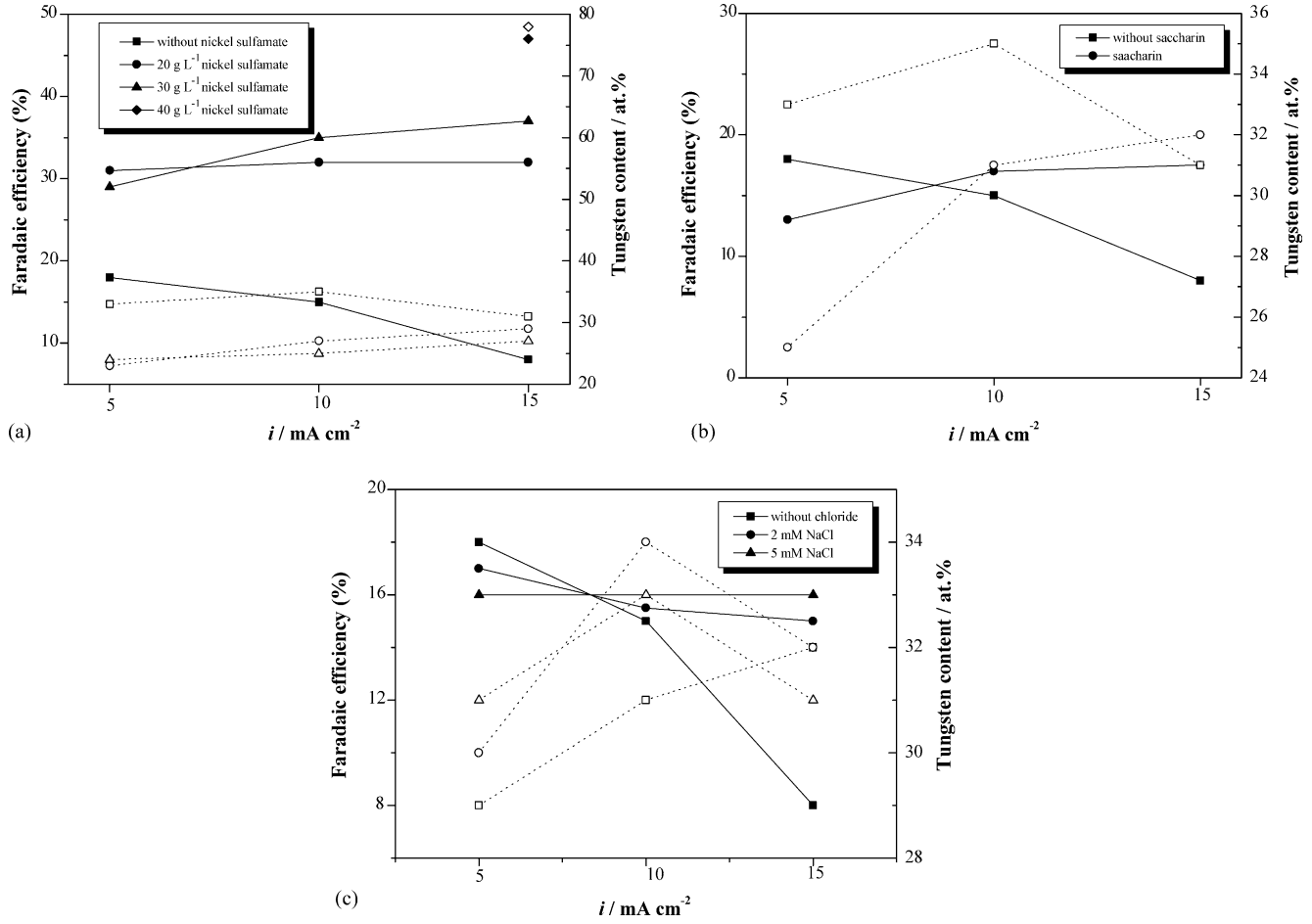

Fig. 2. The effect of additives on the Faradaic efficiency (solid symbols, solid lines) and the deposit tungsten content (empty symbols, dot lines) at different current densities: (a) nickel sulfamate, (b) saccharin, (c) sodium chloride. Nickel sulfate (0.10 M), sodium tungstate (0.40 M), citrate (0.50 M), plating time (6 h), nitrogen purging, and room temperature were kept constant.

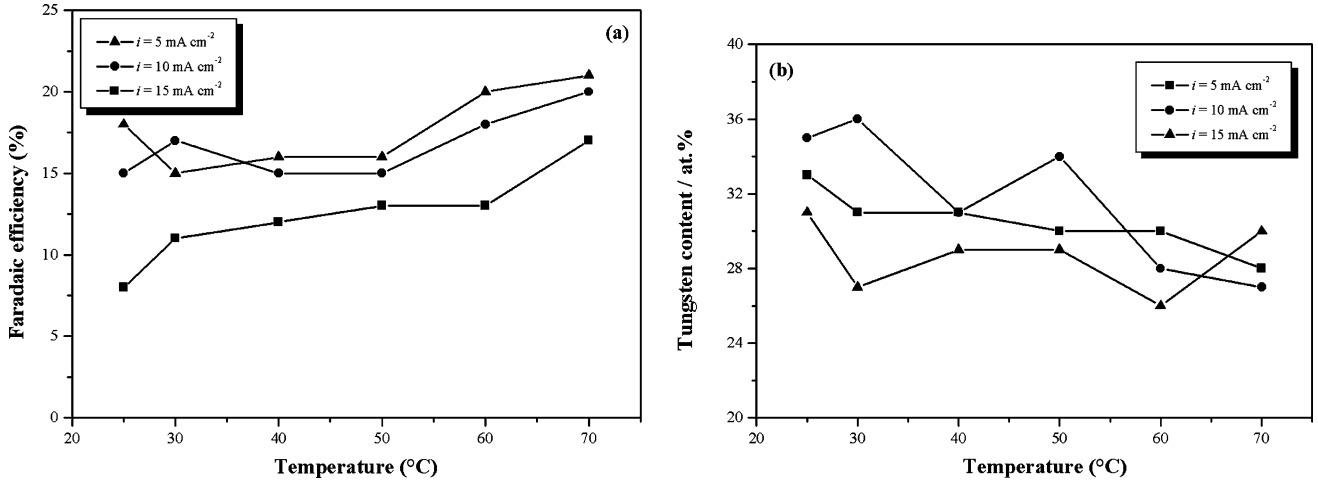

Fig. 3. The effect of temperature on the Faradaic efficiency (a) and the tungsten content of the deposit (b) at different applied current densities. Other variables, including nickel (0.10 M), tungstate (0.40 M), citrate (0.50 M) ions concentration, plating period (6 h), absence of bath additives, and nitrogen purging were kept constant.

increase in the thickness of the coating at a high current density; this will be presented below. When 40 g L^{-1} (124 mM) nickel sulfamate was added, precipitation was noted in solution. This can be associated with the fact that the sum of the molar concentrations of nickel and tungstate ions exceeded that of citrate, following the addition of nickel sulfamate. Hence, the high content of tungsten measured in this case (see Fig. 2a) does not reflect formation of a good Ni–W deposit.

The effect of saccharin (14.6 mM) on the FE in a bath containing 0.10 M Ni^{2+}, 0.40 M WO_4^{2-} and 0.50 M Cit^{3-} and on the tungsten content is shown in Fig. 2b. Saccharin was found to increase the FE at high current densities and decrease the tungsten content of the deposit at low current densities.

The effect of sodium chloride (2–5 mM) on the FE in a bath containing 0.10 M Ni^{2+}, 0.40 M WO_4^{2-} and 0.50 M Cit^{3-} and on the tungsten content is shown in Fig. 2c. This figure shows that chloride additions allow for stabilizing the FE at a nearly constant value for different current densities, the effect being similar when 2 or 5 mM chloride ion is added. In contrast, the FE significantly dropped at high current densities when chloride was absent. Fig. 2c also shows that the addition of chloride ions did not change the composition of the deposit significantly. It should be noted, however, that excess chloride might be harmful to brightness and leveling at the cathode.

Sodium sulfate (25 g L^{-1} = 176 mM) and gelatin (0.5–1%) were also added together. However, gelatin was found to cause foaming. Thus, even when the solution was carefully filtered, no reasonably good coatings were formed. Reviewing the current literature for Ni–W electrodeposits, one may conclude that a surfactant is sometimes added to the bath to ensure that hydrogen gas bubbles, which form on the work piece, are easily liberated by solution agitation [7]. This is useful because hydrogen pitting can be controlled in nickel sulfamate solutions by vigorous agitation. In addition, additives are sometimes used to reduce internal stresses. However, it has been concluded that no single stress reducer decreases the stress at both lower and higher current densities, and that stress reducers often reduce the current efficiency [28].

3.3. The effect of temperature

Temperature is another important variable in the operation of Ni–W plating baths. However, the effect has been reported so far to be mainly on the current efficiency and hardness of the deposit, and less on the tungsten content of the alloy. When the bath contained tartaric acid and boric acid, both the tungsten content and the FE increased with increasing temperature in ammonia-containing baths [29], whereas the effect of temperature on the tungsten content was small in ammonia-free baths [30]. Gileadi and co-workers similarly observed that in ammonia-free solutions, almost no effect of temperature on the tungsten content exists, while the FE increases with temperature [1]. Krishnan et al. [10] also reported an increase in current efficiency with increasing temperature, while Yamasaki et al. [31] described temperature effects both on the tungsten content and the ductility of the deposit. Atanassov et al. [9] observed an increase in the tungsten content with increasing bath temperature both in unstirred and in stirred baths, and explained this behavior in terms of favorable conditions for tungsten transport toward the cathode surface. It was also stated [7] that the deposition rate increased with increasing temperature in the range 54–71 °C.

Based on these observations, it was decided to carry out experiments with varying temperatures from 30 to 70 °C, rather than just at room temperature. Fig. 3 shows the effect of temperature at different current densities on the FE and tungsten content of the deposit, for a bath containing 0.10 M Ni^{2+}, 0.40 M WO_4^{2-} and 0.50 M Cit^{3-}. In general, as the bath temperature was increased, the FE increased. The tungsten content of the deposit did not change much with temperature,

and showed rather irregular behavior, with perhaps some tendency to decrease with increasing temperature. These results are in good agreement with the previous work of Younes and Gileadi [1], keeping in mind that the latter was conducted at a current density of 15 mA cm^{-2} only. More astonishing is the finding of the current work that, in the higher temperature range (50–70 °C), a Ni_4W phase can be formed by electrodeposition. To the best of our knowledge, this is the first ever systematic observation of the ability to form this phase electrochemically. This, however, will be discussed in detail elsewhere [32].

3.4. The effect of current density

The applied current density was varied from 5 to 15 mA cm^{-2} in the present work. Its effects on the FE and tungsten content have already been demonstrated in Figs. 1–3, for baths with different chemistries, additive content, and temperatures. In most cases, the FE decreased when the current density was increased, whereas the tungsten content either increased or passed through a maximum at 10 mA cm^{-2}. At high current densities, where the FE is low, hydrogen evolution becomes more prominent and causes

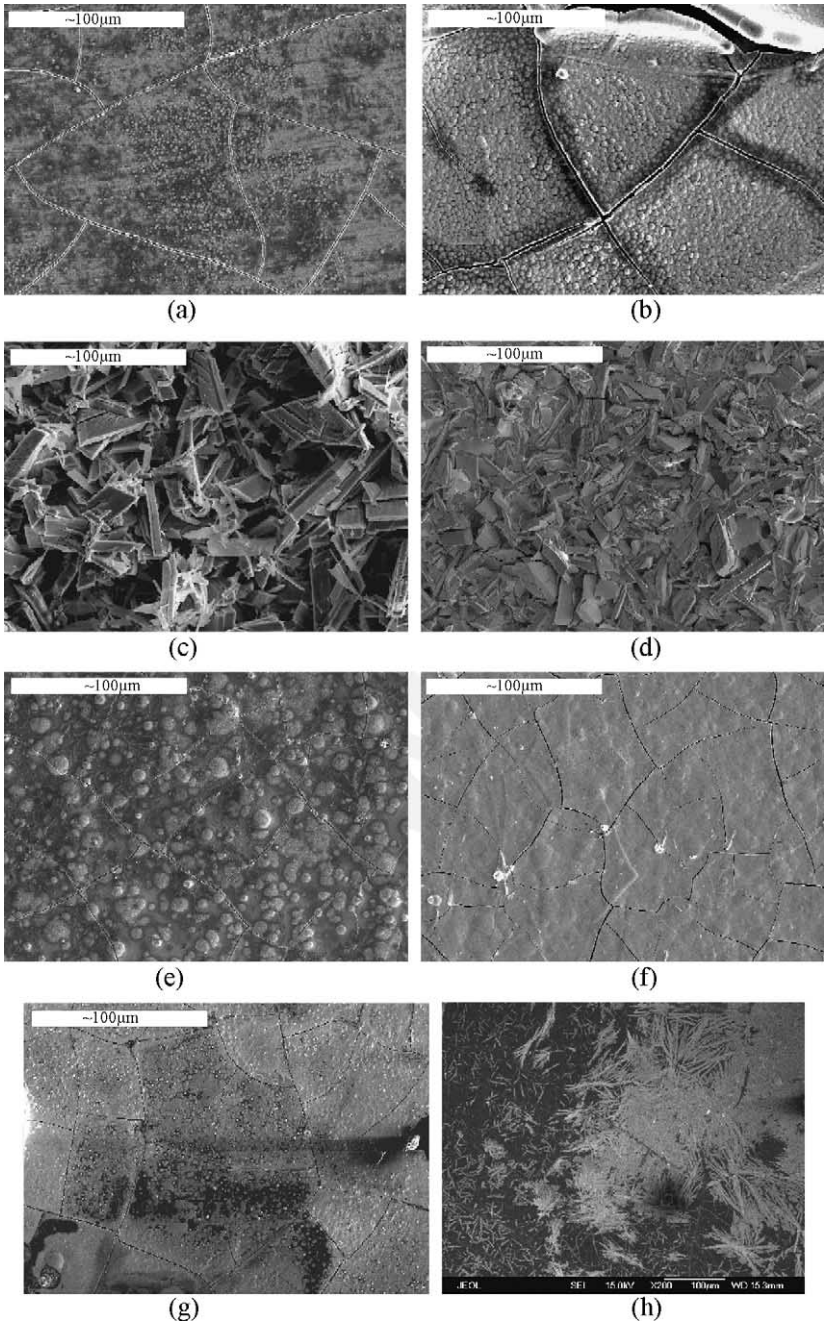

Fig. 4. Scanning electron microscope secondary electron images taken from eight NiW-plated gold samples, representing different process parameters. See text for details.

additional agitation in solution. Moreover, because Ni is deposited easily compared to W, higher FE is expected to result in a higher concentration of Ni. These results indicate some degree of mass transport limitation.

The effect of current density in the Ni–W system has already been studied in the literature. Brenner et al. [33] observed a significant increase in tungsten content with increasing current density in ammonia–citrate bath. Yamasaki et al. [31] reported a similar trend. Atanassov et al. [9] noted a linear increase in tungsten content with increasing current density when vigorous stirring was applied. On the other hand, a maximum was observed at 50–70 mA cm^{-2} in the absence of stirring. At current densities higher than 20 mA cm^{-2}, the FE was 15–40% higher in the stirred bath, where hydrogen evolution was less pronounced, compared to an unstirred bath. Krishnan et al. [10] also monitored a decrease in the FE with increasing current density. Finally, Huang et al. [28] have reported an increase in residual stresses with current density.

3.5. Deposits morphology, cracking pattern and hardness

The surface morphology of the as-deposited samples and their approximate chemical composition were studied by SEM and EDS, respectively. Fig. 4 presents typical SEM images.

Fig. 4a reveals the structure of sample #3 (0.10 M Ni^{2+}, 0.40 M WO_4^{2-} and 0.60 M Cit^{3-}, with nitrogen purging, room temperature, $i = 10$ mA cm^{-2}) that contains 35 at.% W. According to XRD data, this Ni–W alloy has an amorphous structure. A rather dense net of micro-cracks is evident on the surface, which may result either from hydrogen embrittlement or from residual stresses. Donten et al. [34] related similar cracking in amorphous Ni–W deposits mainly to high residual stresses and showed that by incorporation of iron into an alloy deposited on iron-based substrates, this cracking can be eliminated, and both deposit toughness and adhesion can be improved. Close examination of the surface shows that it is consisted of globular regions with gaps in between, and either circular or quasi-circular domain borders. This indicates that no real grain boundaries exist, which supports the prevalence of an amorphous structure. The existence of even smaller globules on top of the larger ones has been observed by others too [2,4].

Fig. 4b demonstrates the structure of sample #5 (0.10 M Ni^{2+}, 0.40 M WO_4^{2-} and 0.50 M Cit^{3-}, with nitrogen purging, room temperature, $i = 15$ mA cm^{-2}) that contains 31 at.% W. It is evident that a combined decrease in the citrate ion concentration and increase in the applied current density result in a similar surface morphology of an amorphous deposit. Some peeling of the deposit off the substrate is also seen in Fig. 4b. One may note the slight decrease in crack density and increase in globules size when compared to Fig. 4a at the same magnification. A similar decrease in crack density with an increase of current density has been reported elsewhere [10].

Fig. 4c shows the structure of sample #17 (0.10 M Ni^{2+}, 0.40 M WO_4^{2-} and 0.25 M Cit^{3-} with nitrogen purging, room temperature, $i = 15$ mA cm^{-2}) that contains 60 at.% W. It should be recalled that precipitation was observed in solution during deposition of this sample. This is most likely the result of the fact that the concentration of citrate is lower than the sum of the concentrations of Ni^{2+} and WO_4^{2-}. Since the amount of citrate in solution is not enough to complex both the nickel and the tungstate ions, precipitation of a salt (probably $NiWO_4$) takes place. Indeed, the SEM micrograph illustrates the presence of a porous crystalline deposit on the surface. Note that in comparison to sample #5, the only change in the deposition process was the reduction of the citrate concentration.

Fig. 4d reveals the structure of sample #32 (0.10 M Ni^{2+}, 0.40 M WO_4^{2-} and 0.40 M Cit^{3-}, with nitrogen purging, room temperature, $i = 15$ mA cm^{-2}) that contains 51–67 at.% W. XRD data showed that this deposit consisted of either the NiW phase or the NiW_2 phase. From the SEM micrograph it is clear that this deposit is crystalline. Furthermore, compared to sample #17 (Fig. 4c), the crystallites seem to be finer and more close-packed. This surface morphology is very different from the smooth scratched surface observed by Zhu et al. [4] for the orthorhombic NiW structure at tungsten contents above 40 at.%. These authors related the scratches to plastic deformation that is initiated in areas of high surface stresses and reported its absence in the fairly ductile fcc phase. It is not clear at this stage whether the morphology observed in the current work can support the formation of the bcc NiW_2 phase, or results from different conditions of both the substrate and plating process.

Fig. 4e demonstrates the structure of sample #38 (0.10 M Ni^{2+}, 0.40 M WO_4^{2-} and 0.50 M Cit^{3-}, without nitrogen purging, room temperature, $i = 15$ mA cm^{-2}) that contains 33 at.% W. This sample was deposited under essentially the same conditions as sample #5 (Fig. 4b), except without nitrogen purging. In general, both the tungsten content and the surface morphology are similar in both cases and represent the formation of an amorphous structure.

Fig. 4f shows the structure of sample #75 (0.10 M Ni^{2+}, 0.40 M WO_4^{2-} and 0.50 M Cit^{3-}, 30 g L^{-1} nickel sulfamate, with nitrogen purging, room temperature, $i = 15$ mA cm^{-2}) that contains 27 at.% W. The only difference from sample #5 (Fig. 4b) is the addition of nickel sulfamate. The resulting surface seems to be smoother, with finer cracks. An optical photomicrograph of the cross-section of this sample is presented in Fig. 5a. The thickness of this deposit was the highest observed in this work (33.0 ± 1.0 μm), as compared to all other baths without additives where the coating thickness was less than 10.0 μm. This finding is in accordance with the high FE measured for this sample (Section 3.2, Fig. 2a). However, sample #75 was also softer than the other ones, exhibiting hardness of 450 ± 28 VHN. In Section 1 it was mentioned that the hardness of as-plated Ni–W alloys is typically in the range 650–750 VHN [7,8]. In addition, Donten et al. [14] reported hardness values in the range 700–800 VHN. As a rule

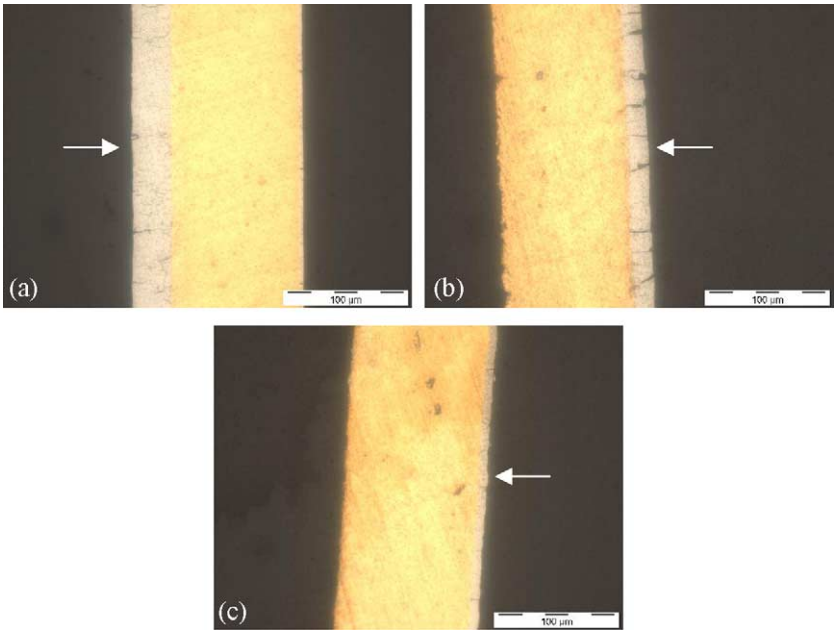

Fig. 5. Optical microscope images showing the metallographic cross-sections of three NiW-plated gold substrates. The plated side is marked by an arrow. Different coatings thicknesses and cracking appearance are evident. See text for details.

of thumb, it is accepted that lower residual stresses in electroformed Ni–W (and other) alloys result in a corresponding decrease in hardness as well as in cracking [28]. Therefore, in view of the reduced residual stresses expected due to the addition of nickel sulfamate (see Section 2.1), it is not surprising that the measured hardness values are fairly low. It is possible, however, that a subsequent heat treatment will raise the hardness of this deposit to desired levels.

Fig. 4g demonstrates the structure of sample #84 (0.10 M Ni^{2+}, 0.40 M WO_4^{2-}, 0.50 M Cit^{3-}, 33.4 mM saccharin, with nitrogen purging, room temperature, $i = 15\,mA\,cm^{-2}$) that contains 32 at.% W. It would seem that the addition of saccharin did not change the surface morphology significantly, although the micro-cracks may have become slightly finer. However, an optical photomicrograph of the cross-section of this sample reveals (Fig. 5b) that the thickness of this coating ($17.2 \pm 0.3\,\mu m$) is larger than that of coatings produced from baths without additives. This observation is consistent with the higher FE of deposition from a saccharin-containing bath at $15\,mA\,cm^{-2}$ (Section 3.2, Fig. 2b). The change in FE may also explain the difference in coating thickness between the nickel sulfamate- and saccharin-containing baths. Yet, as compared to sample #75, the hardness of sample #84 increased significantly to 768 ± 64 VHN. Brown introduced the use of benzene sulfonamides and sulfonimides, including saccharin, in electrodeposition and indicated the prime importance of the non-saturation of the benzene ring [16]. The use of a ductility agent, which contains less than 10% benzene sulfonamide, in order to reduce the "as-plated" stresses and cracking of the Ni–W deposit was recommended in the literature [7,35]. This was related to a decrease in the amount of absorbed hydrogen. The ductility agent was also reported to stabilize the amorphous phase compared to the microcrystalline fcc phase. In another study [17], saccharin was found to strongly affect the morphology evolution of electrodeposited nickel films on gold only at high overpotentials, while not disturbing it at low overpotentials.

Experiments were also conducted to study the effect of plating bath temperature on the structure and properties of the coating. All of these experiments were carried out in the same bath (0.10 M Ni^{2+}, 0.40 M WO_4^{2-} and 0.50 M Cit^{3-}, with nitrogen purging), at temperatures in the range of 50–70 °C, applied current densities (5–15 mA cm^{-2}), and deposition periods (6–24 h). Samples #87, 88 and 89 were all coated at 50 °C for 6 h, but at different current densities of 15, 10 and 5 mA cm^{-2}, respectively. The tungsten contents of these deposits were estimated by EDS as 31, 30 and 21 at.%, respectively. From these data it seems that a Ni_4W phase was formed only at the lowest current density (sample #89). The thickness and hardness of this coating were measured on a cross-section and found to be $8.7 \pm 0.1\,\mu m$ and 668 ± 43 VHN, respectively.

Samples #93, 94 and 95 were all coated at a higher temperature of 60 °C for 6 h, at three different current densities of 15, 10 and 5 mA cm^{-2}, respectively. The surface morphology of sample #93 was found to be non-uniform; the chemical composition of this sample was also non-uniform, with tungsten content varying from about 17 to 24 at.%, to as high as 32 at.% in different areas. The chemical compositions of samples #94 and #95 were also relatively non-uniform, with tungsten contents varying in the range of 25–30 and 26–34 at.%, respectively. Fig. 4h shows typical morphology of sample #95. The thickness of this sample was measured on a cross-section and found to be $5.5 \pm 0.3\,\mu m$. In order to assess the effect of

deposition period, two samples (#96 and #97) were coated under conditions identical to those of sample #95, but for 24 and 12 h, respectively. The tungsten content in these two deposits was estimated as 20 and 22 at.%, respectively. These two coatings were more morphologically and chemically uniform compared to sample #95, and their composition clearly resembled that of Ni_4W. The coating thickness was found to increase almost linearly with deposition period, attaining 24.8 ± 0.6 μm after 24 h (sample #96). This allowed also more reliable measurements of deposit hardness, yielding a

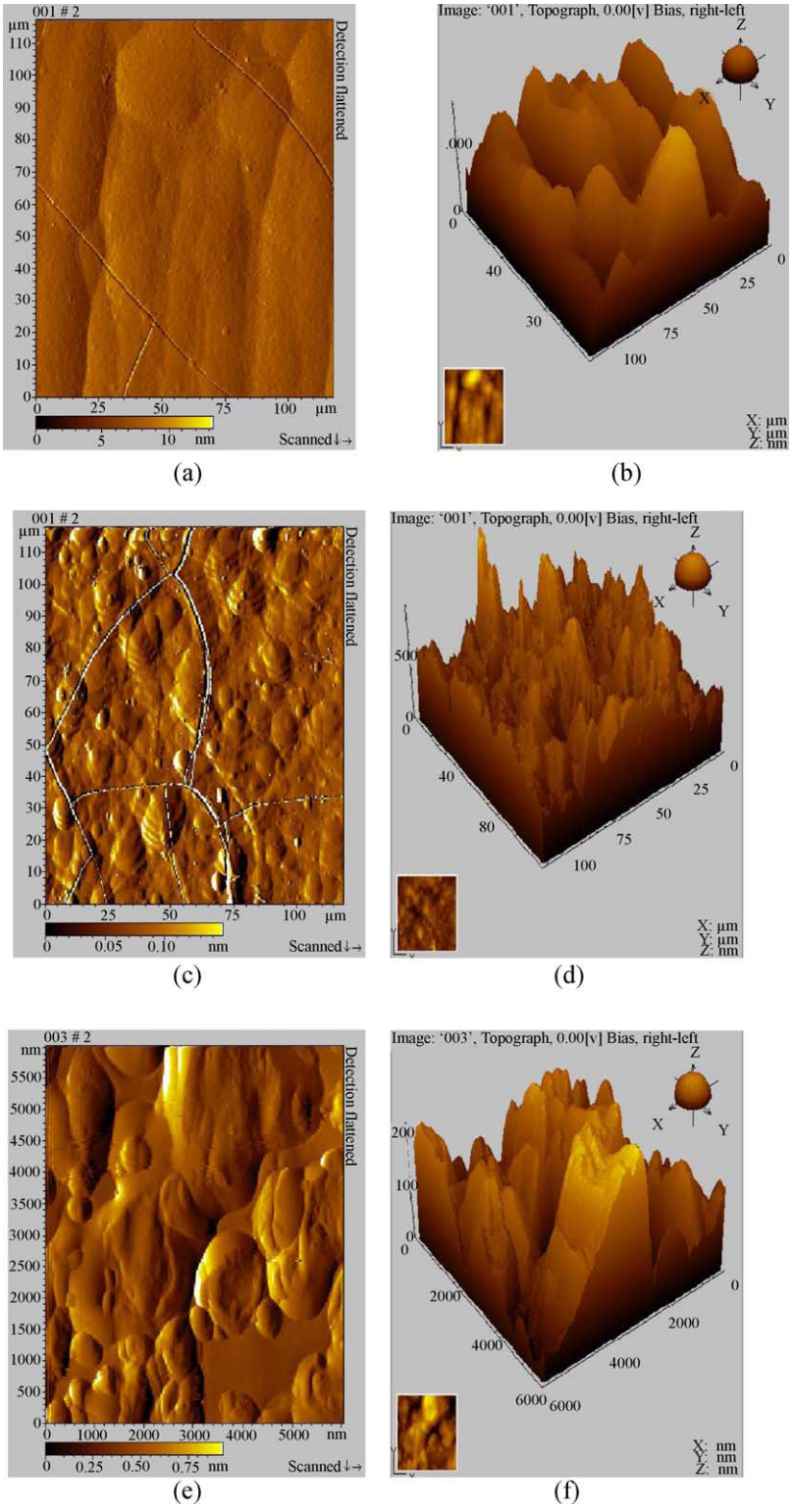

Fig. 6. Atomic force deflection and 3D images from three NiW-plated gold samples, representing different process parameters. See text for details.

value of 577 ± 44 VHN for sample #96. When comparing to sample #89, one may conclude that by raising the bath temperature from 50 to 60 °C, the hardness of the deposit decreased. This observation is similar to that of Atanassov et al. [9], who reported a maximum in hardness of about 720 VHN at 50 °C under unstirred conditions. Yamasaki et al. [31], on the other hand, reported an increase in hardness from 602 to 770 VHN when the bath temperature was raised from 60 to 90 °C. The same group also observed [36] that the crack density generally decreases with an increase of temperature, and that cracking could be eliminated at 70 °C for any current density. However, this is somehow puzzling because, as aforementioned, cracking typically increases in harder Ni–W electrodeposits.

Finally, samples #90, 91 and 92 were all plated at 70 °C for 6 h, but at different current densities of 15, 10 and 5 mA cm^{-2}, respectively. The tungsten contents of these deposits were estimated as 32, 33 and 22 at.%, respectively. Once again, only the combination of a low current density and a high temperature seems to enable the formation of a Ni_4W phase. Fig. 5c shows an optical photomicrograph of the cross-section of sample #92, on which a deposit thickness 5.9 ± 0.1 μm was measured.

The surface morphology of several as-deposited alloys was also studied by AFM. Selected images are presented here. Fig. 6a and b shows the two-dimensional (2D) deflection image and the three-dimensional (3D) topography image, respectively, of sample #69 (0.05 M Ni^{2+}, 0.40 M WO_4^{2-}, 0.50 M Cit^{3-}, no additives, with nitrogen purging, room temperature, $i = 10\,mA\,cm^{-2}$) that contains 37 at.% W. The scan area here is fairly large (117 μm × 117 μm). The deflection image, also known as the error signal image, results from inability of the electronics feedback circuit to maintain a constant force. It represents the gradient of shape change via differentiation, and is thus more sensitive to delegate spatial information such as sharp edges. Note that the *z*-axis in the 3D image is of a nm scale. In Fig. 6a and b, surface cracking as well as the absence of a periodic structure are evident. The presence of random humps also supports the existence of an amorphous structure. It should be noted that in some other areas on this sample, there were indications of the existence of local crystalline structures.

Fig. 6c and d shows the deflection and 3D images, respectively, of sample #75. SEM and cross-section optical photomicrographs of this sample have already been presented in Figs. 4f and 5a, respectively. The scan area here is 117 μm × 117 μm too. Cracking is clearly evident at the surface. Yet, the addition of nickel sulfamate resulted in a reduced surface roughness and a significantly higher density of aggregates. When the current density was reduced from 15 to 5 mA cm^{-2} for the same bath composition of nickel sulfamate (30 g L^{-1}), AFM images showed higher tendency for crystallinity. This finding may be related to the decrease in tungsten content, as evident from Fig. 2a, towards the lower limit of 20 at.% for which an amorphous phase has been observed. A higher tendency to crystallinity was also noticed when the nickel sulfamate content of the bath was reduced from 30 to 20 g L^{-1} under otherwise the same conditions. This is illustrated in Fig. 6e and f for sample #79 (0.10 M Ni^{2+}, 0.40 M WO_4^{2-}, 0.50 M Cit^{3-}, with nitrogen purging, room temperature, $i = 15\,mA\,cm^{-2}$) that contains 29 at.% W. Note that the scan area in this case is only 6 μm × 6 μm. SEM images from this sample also indicated the presence of crystalline platelets at the surface.

4. Summary and conclusions

This work demonstrated the effect of bath chemistry, additives and operating conditions on the Faradaic efficiency (FE), chemical composition, surface morphology, cracking pattern, thickness and hardness of Ni–W alloys deposited on stationary working electrodes from citrate-containing open baths in the absence of ammonia or ammonium salts. All plating baths consisted of nickel sulfate, sodium tungstate and trisodium citrate. The following conclusions were drawn and discussed with respect to a comprehensive literature survey on electrodeposition of Ni–W alloys:

(1) The FE is increased with either increased concentration of Ni^{2+}, decreased concentration of Cit^{3-}, decreased current density, or addition of nickel sulfamate.
(2) The tungsten content in the alloy is increased as the concentration of Cit^{3-} is increased at a low current density, or as the concentration of Cit^{3-} is decreased at a high current density.
(3) When the Ni^{2+} concentration is reduced to 0.01 M, poor deposits are formed.
(4) Addition of nickel sulfamate results in a remarkable increase of the Faradaic efficiency (and hence, of deposit thickness for the same deposition time and applied current), a slight decrease in its tungsten content, reduced residual stresses, a significant decrease in hardness, and a reduced surface roughness on the micrometeric scale.
(5) Addition of saccharin results in increased FE and deposit thickness at high current densities, and a decreased tungsten content of the deposit at low current densities.
(6) Additions of chloride stabilize the FE at a nearly constant value for each current density, without changing the composition of the deposit. At 15 mA cm^{-2}, the presence of chlorides increases the FE significantly.
(7) As the bath temperature is increased, the FE is increased but the tungsten content of the alloy remains approximately constant, with perhaps a small tendency to decrease. Temperatures in the range of 50–70 °C allow formation of a Ni_4W phase.
(8) Crack density is typically decreased when the current density is increased.

Acknowledgements

The authors wish to thank Mr. M. Levenshtein and Mr. M. Eliyahu for their help with hardness and AFM measurements, respectively. The fruitful discussions with Mr. B. Tal are also acknowledged. T.M. Sridhar is thankful to the Pikovsky Valachi Foundation, Tel-Aviv University, for providing him with a postdoctoral scholarship.

References

[1] O. Younes, E. Gileadi, Electrochem. Solid-State Lett. 3 (12) (2000) 543.
[2] O. Younes, L. Zhu, Y. Rosenberg, Y. Shacham-Diamand, E. Gileadi, Langmuir 17 (2001) 8270.
[3] O. Younes, E. Gileadi, J. Electrochem. Soc. 149 (2) (2002) 100.
[4] L. Zhu, O. Younes, N. Ashkenasy, Y. Shacham-Diamand, E. Gileadi, Appl. Surf. Sci. 200 (1–4) (2002) 1.
[5] O. Younes-Metzler, L. Zhu, E. Gileadi, Electrochim. Acta 48 (18) (2003) 2551.
[6] S. Yao, S. Zhao, H. Guo, M. Kowaka, Corrosion 52 (3) (1996) 183.
[7] PWA 36975: Electroplated NiW—thin deposit (Enloy Ni-500). http://www.enthone.com.
[8] P. Schloßmacher, T. Yamasaki, Mikrochim. Acta 132 (2000) 309.
[9] N. Atanassov, K. Gencheva, M. Bratoeva, Plat. Surf. Finish. 84 (2) (1997) 67.
[10] R.M. Krishnan, C. Joseph Kennedy, S. Jayakrishnan, S. Sriveeraraghavan, S.R. Natarajan, P.G. Venkatakrishnan, Met. Finish. 93 (7) (1995) 33.
[11] L. Namburi, Electrodeposition of NiW Alloys into Deep Recess, M.Sc. Thesis, Louisiana State University, December 2001.
[12] N. Suliţanu, J. Magn. Mater. 231 (2001) 85.
[13] N.D. Suliţanu, Mater. Sci. Eng. B 95 (2002) 230.
[14] M. Donten, Z. Stojek, H. Cesiulis, J. Electrochem. Soc. 150 (2) (2003) 95.
[15] L. Cambi, R. Piontelli, Rend. Inst. Lombardo Sci. 72 (1938) 128.
[16] F.A. Lowenheim (Ed.), Modern Electroplating, 3rd ed., John Wiley and Sons, Inc., New York, NY, 1974.
[17] D.C. Dibble, A.A. Talin, J.J. Kelly, The effect of saccharin on electrodeposited nickel: an in situ SPM study, J. Electrochem. Soc., in press.
[18] D.J. Kim, M.H. Seo, J.S. Kim, Materials properties of Ni–P–B electrodeposits, J. Electrochem. Soc., in press.
[19] G. Di Bari, ASM Handbook, vol. 5: Surface Engineering, ASM International, Materials Park, OH, 1994, p. 201.
[20] K.B. Lebedev, The Chemistry of Rhenium, Butterworths, London, UK, 1962.
[21] K. Boto, Electrodep. Surf. Treatment 3 (1975) 77.
[22] M. Donten, J. Solid State Electrochem. 3 (2) (1999) 87.
[23] M. Obradović, J. Stevanović, R.J. Stevanović, A. Despić, J. Electroanal. Chem. 491 (1/2) (2000) 188.
[24] H. Cesiulis, A. Baltutiene, M. Donten, M.L. Donten, Z. Stojek, J. Solid State Electrochem. 6 (4) (2002) 237.
[25] W.H. Safranek, The Properties of Electrodeposited Metals and Alloys, 2nd ed., American Electroplaters and Surface Finishers Society, Orlando, FL, 1986, p. 348.
[26] A. Brenner, Electrodeposition of Alloys, vol. 2, Academic Press, New York, NY, 1963, p. 403.
[27] C.-H. Huang, Plat. Surf. Finish. 84 (4) (1997) 62.
[28] C.-H. Huang, W.Y. She, H.M. Wu, Plat. Surf. Finish. 86 (12) (1999) 79.
[29] T.F. Frantsevich-Zabludovskaya, A.I. Zayats, Zh. Prikl. Khim. 30 (1957) 723.
[30] H. Offermanns, M.V. Stackelberg, Metalloberflaeche 1 (1947) 142.
[31] T. Yamasaki, R. Tomohira, Y. Ogino, P. Schloßmacher, K. Ehrlich, Plat. Surf. Finish. 87 (5) (2000) 148.
[32] T.M. Sridhar, N. Eliaz, E. Gileadi, Electrochem, Solid State Lett., in press.
[33] A. Brenner, P.S. Burkhead, E. Seegmiller, J. Res. Natl. Bur. Stand. 39 (1947) 351.
[34] M. Donten, H. Cesiulis, Z. Stojek, Electrochim. Acta 45 (2000) 3389.
[35] W.J. Wieczerniak, S. Martin, US Patent 5,525,206 (11 June 1996), Brightening additive for tungsten alloy electroplate.
[36] T. Yamasaki, P. Schloßmacher, K. Ehrlich, Y. Ogino, Mater. Sci. Forum 269 (1998) 975.